*36th EPS Conference on Plasma Phys. Sofia, June 29 - July 3, 2009 ECA Vol.**33E**, P-2.161 (2009)*

Coupling between JET Pedestal n_e-T_e and Outer Target Plate Recycling: Consequences for JET ITER-Like-Wall Operation

K McCormick[1], G Maddison[2], C Giroud[2], M Beurskens[2], A Boboc[2], S Brezinsek[3], T Eich[1], W Fundamenski[2], S Jachmich[4], M Stamp[2], H Thomsen[1] and JET EFDA contributors*

JET-EFDA, Culham Science Centre, OX14 3DB, Abingdon, UK

[1] Max-Planck IPP, EURATOM Association, D-85748 Garching, Germany.

*[2] EURATOM/UKAEA Fusion Association, Culham, Abingdon, Oxon. OX14 3DB, UK.**

[3] FZ Jülich GmbH, Institut für Plasmaphysik, Association EURATOM-FZJ, Jülich, Germany.

[4]Laboratory for Plasma Physics, ERM/KMS, EURATOM-Association Belgian-State, Brussels, Belgium

Introduction: With the tungsten target plates of the JET ITER-Like-Wall (ILW) phase, carbon radiation will be reduced and must be replaced by that of seeded impurities to prolong target plate lifetime. Investigations to this end of ELMy-H (EH) & Advanced Tokamak (AT) scenarios using N_2 and Ne along with D_2 fuelling have been carried out in matrix fashion (fig. 1, top), whereby the aim was to cover a large variation in divertor power loading P_{div} and temperature T_e^{div} regardless of core performance. The intended effect of impurity seeding is to increase radiation P_{rad} in order to mitigate P_{div} and that of D_2 to enhance recycling to further reduce T_e^{div}, both being necessary for ILW-compatibility. P_{rad}/P_{in} ranged over 48-66% (EH) and 31-60% (AT). Details on P_{rad} and P_{div} are given in a companion paper /1/. This data set is used to study the interrelationships between the pedestal temperature T_e^{ped} & density n_e^{ped} and the ion flux Γ_i to the outer target plate. An advantage of these studies is the wider range of n_e^{ped} and T_e^{ped} afforded by the use of impurities (fig. 2). Different type-I ELM regimes also prevail: For EH, ν_{ELM} initially decreases with D_2 (~20->10Hz). Impurities can provoke compound ELMs ($\nu_{ELM} \geq$ 3Hz) as well as augment ν_{ELM} (to 50Hz).

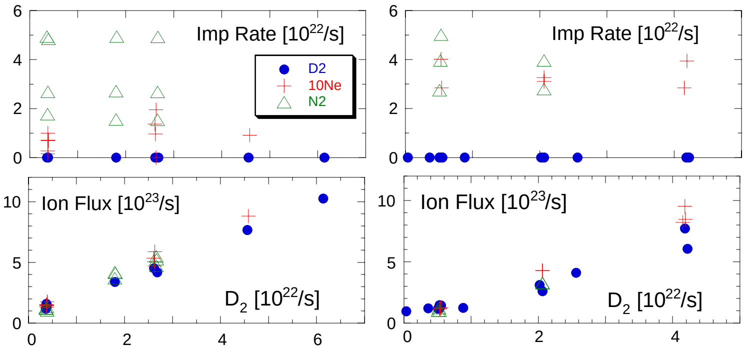

Fig. 1:Impurity electron rate & ion flux to the outer target plate vs D_2 electron rate. Ne-rate multiplied by 10. Left ELMy-H; Right AT.
EH: *~16MW, 2.5MA, 2.7T, q_{95}~3.5, n_{eGW}~0.65-1.07, $H_{98y,2}$~0.8-1.09;*
AT: *~23MW, 1.75MA, 2.7T, q_{95}~5, n_{eGW}~0.41-0.79, $H_{98y,2}$~0.66-1.02.*
NBI electron fuelling ~1.1 10^{21}/s (EH) & 1.8 10^{21}/s (AT).

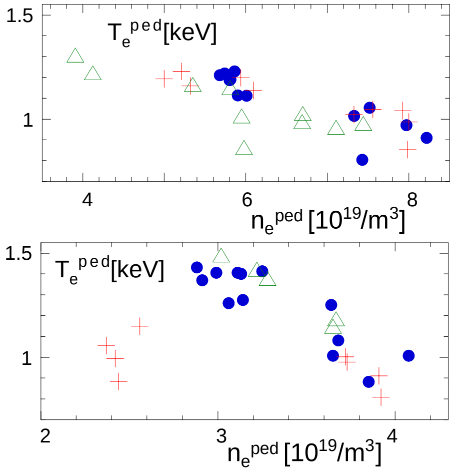

Fig. 2:Pedestal T_e^{ped} vs n_e^{ped} . dot = D_2 fuelling, plus=D_2+Ne, triangle=D_2+N_2 Top ELMy-H; Bottom AT

---

[*] See the Appendix of F. Romanelli et al., Fusion Energy Conference 2008 (Proc. 22nd Int. FEC Geneva, 2008) IAEA, (2008)

ν_{ELM} (AT) largely spans the range ~50 - 200Hz increasing with D_2 for the subset selected.

2. Experimental Results: All quantities reported are averaged over ~1s, i.e. over many ELM cycles. This is readily done using T_e from the ECE radiometer, with the values deviating less than 50eV (<5%) from those gained from the High Resolution Thomson Scattering (HRTS) system. As radiometer values were not always available, T_e from HRTS is cited, read at the 90% flux surface. Inter-ELM T_e-excursions in compound ELM phases can more than 200eV (only with Ne in EH) with an average deviation from the mean of <±100eV, otherwise ~±50eV. The edge vertical interferometer channel (tangent to 90% flux surface) also enables good time averaging, has a low noise level and none of the potential calibration uncertainties associated with Thomson scattering. It is very closely related to n_e from HRTS and is taken to define n_e^{ped}, with a typical uncertainty of $\pm 10^{18}$ m^{-3}. A rough estimate of Γ_i is obtained from the D_α line intensity summed over the outer target plate $\Phi_{D\alpha}$ using S/XB~30, i.e. $\Gamma_i = 30\ \Phi_{D\alpha}$. An estimate of T_e^{div} is derived from P_{div}^{out} (IR camera) and Γ_i: $T_e^{div} = P_{div}^{out}/(8\Gamma_i x1.610^{-19})$, 8=energy transmission factor. Langmuir probe results from other EH discharges indicate this quantity need be multiplied by 2 to obtain the peak T_e. Values for T_e^{div}, energy confinement time τ_E, T_e^{ped} and n_e^{ped} are plotted vs. Γ_i in fig. 3. Note, Γ_i is largely determined by D_2 (fig. 1).

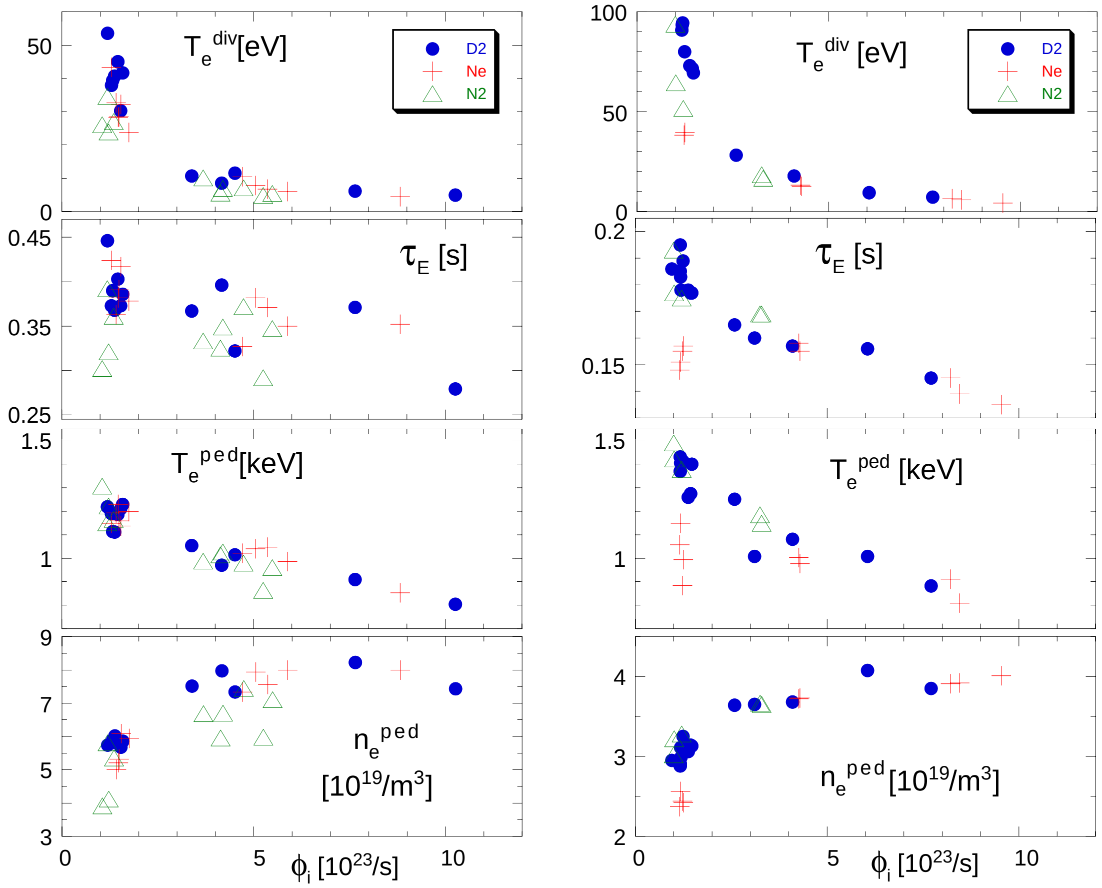

Fig. 3: top to bottom, all vs. ion flux to target plate Γ_i: T_e^{div} computed from P_{div}^{out} & Γ_i using $T_e^{div} = 2 P_{div}^{out}/(8 \times e \times \Gamma_i)$; energy confinement time τ_E,; T_e^{ped} & n_e^{ped}. Left ELMy-H; Right AT.

Higher Γ_i means lower τ_E, with impurities often making matters worse (fig. 3), in particular at lowest Γ_i where a dramatic drop in n_e^{ped} can occur (also in T_e^{ped} for AT Ne-seeding), associated with an impurity-driven increase in ν_{ELM}. Seeded Ne or N_2 leads to an obvious enhancement of P_{rad} only at lower Γ_i (-> lower D_2) for the present carbon-dominated environment (50->61% for EH, 30->60% for AT) /1/. Evidently T_e^{ped} is not reduced by P_{rad} cooling as one might expect (fig. 3); it does decrease uniformly with higher Γ_i, showing minor impurity variations. In contrast, n_e^{ped} initially increases with Γ_i (D_2 fuelling), then rolls over.

3. Discussion: SOLPS code calculations for a density scan at constant power (5MW, inner & outer strike points on horizontal target) may be used to examine how the values of $\Phi_{D\alpha}^{code}$ and Γ_i^{code} are related /2/. The result is for T_e^{div}>4eV $\Phi_{D\alpha}$~$\Gamma_i^{0.76}$, i.e. $S/XB = \Gamma_i^{code}/\Phi_{D\alpha}^{code}$ is not constant (due in part to the S/XB T_e dependence). Nonetheless, D_α^{code} still mirrors Γ_i^{code} over a wide range of T_e^{div}, implying that the assumption S/XB=30 is a credible approach to gain a first estimate of the experimental Γ_i from the measured $\Phi_{D\alpha}$. Taking the separatrix density n_{es} from HRTS, using a Tanh fit in the gradient region and assuming the separatrix position is correctly given by EFIT, yields the relationship Γ_i~$n_{es}^{2.5\pm0.3}$ for both EH & AT. This signifies that Γ_i is a very sensitive probe for changes in n_{es}, n_{es} being more difficult to measure with precision due to the steep gradients in the edge region and uncertainty in separatrix location.

Fig. 4 illustrates that Γ_i (e.g. n_{es}) is closely correlated with n_e^{ped}/τ_E, meaning an enhancement in Γ_i dictates an increase in n_e^{ped} and/or a decrease in τ_E must prevail (τ_E is intertwined with the D_2- & impurity-levels). Another correlation exists between Γ_i and n_e^{ped}/T_e^{ped} (fig. 4). A least-squares regression (not accounting for errors in n_e^{ped} & T_e^{ped}) yields good fits (given in the fig. 5 caption) to Γ_i over the entire operational ranges for both ELMy-H and AT scenarios.

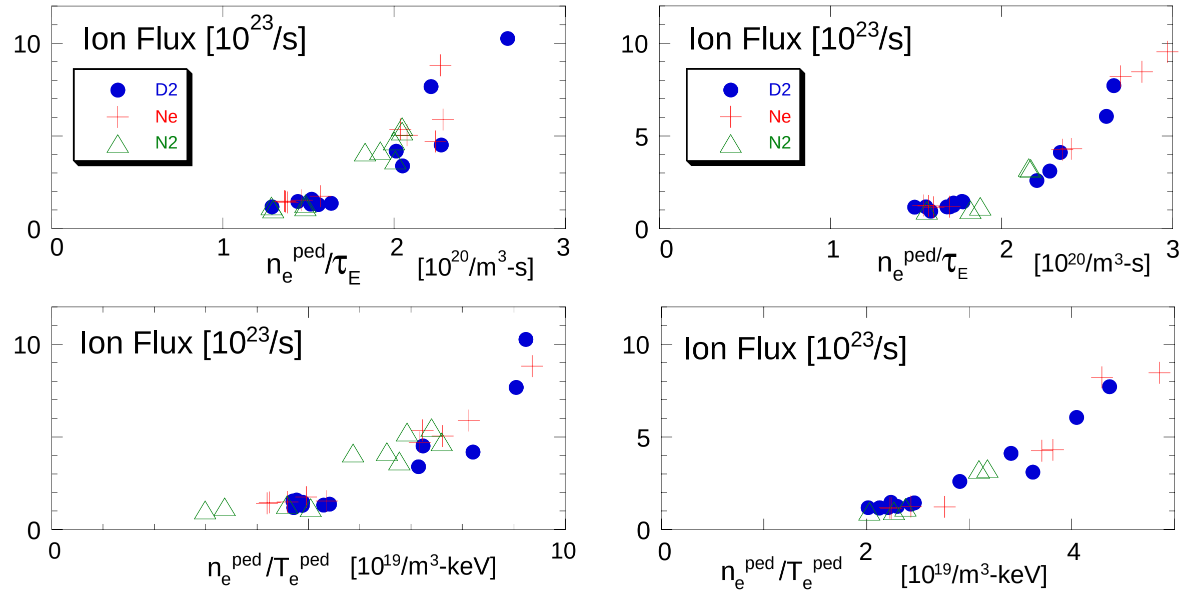

Fig. 4: Ion Flux Γ_i to outer target plate vs. n_e^{ped}/τ_E (top) & n_e^{ped}/T_e^{ped} (bottom). Left ELMy-H; Right AT.

These encompass an order of magnitude change in Γ_i and a factor of ~2 for n_e^{ped}-T_e^{ped}. The exact form of the fits is not of importance here, rather the demonstration of the very coherent interplay among τ_E-n_e^{ped}-T_e^{ped} and Γ_i, illustrated in figs. 4 and 5, i.e. a coupling over the edge transport barrier (ETB) region between the core/pedestal and Γ_i to the outer target plate (and thus n_{es}). In addition, the estimated n_{es} values won from HRTS are found to be nearly linear with n_e^{ped}/τ_E for both EH & AT (not shown). These are new observations of fundamental nature, implying that any change in Γ_i is automatically accompanied by a change in τ_E-n_e^{ped}-T_e^{ped} along the operational curves defined by the points of figs. 4 & 5 and vice versa.

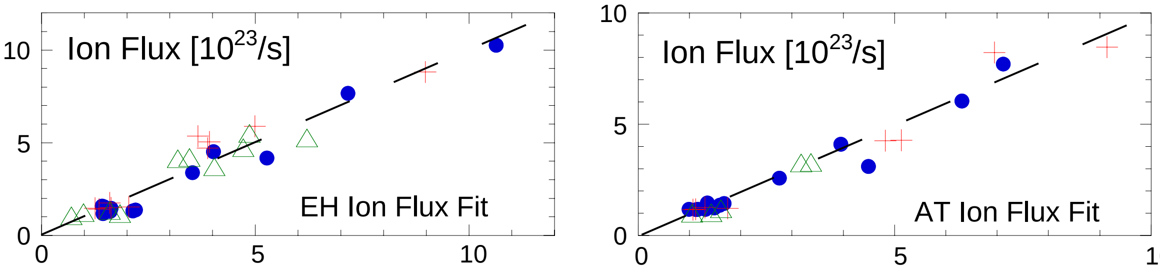

Fig. 5: Γ_i *vs fit: Left ELMy-H* $(9.3 10^{13}\, n_e^{ped1.11\pm0.35}/T_e^{ped4.13\pm0.54})$*; Right AT*$(1.17 10^{-30}\, n_e^{ped3.08\pm0.21}/T_e^{ped2.22\pm0.18})[m^{-3}, eV]$

4. Conclusions: The discovered link among τ_E-n_e^{ped}-T_e^{ped} and Γ_i (e.g. n_{es}) suggests a phenomenon such as “stiff profiles“ could be in action in the ETB, perhaps in combination with a critical gradient related to ELM onset conditions. This remains to be examined. Stiff ETB profiles have been observed on ASDEX-Upgrade, with η_e~2 being common /3/. In any case, the observed coupling, whatever its origin, has ramifications when producing ILW-compatible conditions at the target plate: Enhanced Γ_i will be obligatory to suppress T_e^{div} to tolerable levels (exact value to be determined at the start of ILW operation) and also to secure reasonable plasma operation in the presence of mandatory seeded impurities. Higher Γ_i is achievable only through D_2 fuelling - leading to higher n_{es} - and through the coupling to higher n_e^{ped}/τ_E or n_e^{ped}/T_e^{ped}. This chain of events appears unavoidable.

A corollary is that the increase in neutral pressure associated with higher D_2 does not necessarily lead to a lower τ_E because of penetration to the pedestal and reduction of T_e^{ped}. Rather, the change in pedestal parameters is a result of constraints imposed by the established interconnections in association with the change in n_{es}. Similarly, an alteration in pedestal confinement – due to modes, for example, present in some of the selected discharges /1/ or due to the addition of impurities – will also effect a modification of n_{es} and Γ_i.

5. References

1. G Maddison et al., Paper P2.160 this conference
2. D Coster, private communication
3. A Kallenbach et al., NF **43** (2003) 573; J.Neuhauser et al.,PPCF **44** (2002) 855

This work, supported by the European Communities under the contract of Association between EURATOM and the Max-Planck IPP, was carried out within the framework of the European Fusion Development Agreement. The views and opinions expressed herein do not necessarily reflect those of the European Commission.